Nuclear Instruments and Methods in Physics Research B 379 (2016) 73–77

Contents lists available at ScienceDirect

Nuclear Instruments and Methods in Physics Research B

journal homepage: www.elsevier.com/locate/nimb

Ion beam induced cubic to monoclinic phase transformation of nanocrystalline yttria

N.J. Shivaramu [a,b], B.N. Lakshminarasappa [a,*], K.R. Nagabhushana [c], Fouran Singh [d]

[a] Department of Physics, Bangalore University, Bangalore 560 056, India
[b] Department of Physics, Indian Academy Degree College, Bangalore 560 043, India
[c] Department of Physics (S & H), PES University, Bangalore 560 085, India
[d] Inter University Accelerator Centre, P.O. Box No. 10502, New Delhi 110 067, India

ARTICLE INFO

Article history:
Received 12 November 2015
Received in revised form 12 March 2016
Accepted 6 April 2016
Available online 13 April 2016

Keywords:
Y_2O_3 nanocrystal
XRD
HR-TEM
Raman spectroscopy
Phase transformation

ABSTRACT

Sol gel derived nanocrystalline yttria pellets are irradiated with 120 MeV Ag^{9+} ions for fluence in the range 1×10^{12}–3×10^{13} ions cm^{-2}. Pristine and irradiated samples are characterized by X-ray diffraction (XRD), transmission electron microscopy (TEM) and Raman spectroscopy. XRD pattern of pristine Y_2O_3 nanocrystal reveal cubic structure. A new XRD peak at 30.36° is observed in pellet irradiated with 1×10^{13} ions cm^{-2}. The peak at 30.36° is corresponding to $(40\bar{2})$ plane of monoclinic phase. The diffraction intensity of $(40\bar{2})$ plane increases with Ag^{9+} ion fluence. Raman spectrum of pristine pellet show bands corresponding to cubic phase. And, ion irradiated sample show new peaks at 410, 514 and 641 cm^{-1} corresponding monoclinic phase. HR-TEM and SAED pattern of ion irradiated sample confirmed the presence of monoclinic phase. Hence, it is confirmed that, 120 MeV Ag^{9+} ions induce phase transformation in nanocrystalline Y_2O_3.

1. Introduction

Recently nanocrystalline yttrium oxide (Y_2O_3) attracted extensive research interest due to its unique optical, electrical, chemical and thermal properties. Y_2O_3 finds wide usage in a many luminescent host materials, medical diagnostics as well as biological, industrial and research fields [1–3]. Cubic phase of Y_2O_3 exhibit wide transparent range from UV (220 nm) to infrared (~8 μm) region, it is optically isotropic and hard, having high refractive index (~1.92). It possess high corrosion resistivity, high radiation stability, high melting point (~2723 K), large band gap (5.72 eV) and low phonon energy (~380 cm^{-1}) which leads to very narrow emission and enhanced quantum efficiency [4,5].

Y_2O_3 exist in cubic (C-type), monoclinic (B-type) and hexagonal (A-type) structures. C-type structure is stable at room temperature and normal pressure. Under high temperature or pressure, the C-type will be compressed and leading to reduction in the Y–O bond length. Thus, the cubic structure will lose stability and atoms will rearrange to form a higher density phase [6]. Hence, it is important to study the phase formation of different polymorphs in nano size regimes in particular cubic to monoclinic phase transition.

Swift heavy ions (SHI) have been explored by researchers in different ways in the field of material science. The energy of the ion, ion fluence and ion species greatly affect the structural properties of materials. SHI penetrates deep into the target material; lose their energy predominately through inelastic collisions with the target electrons. The resulting intense electronic excitation can produce a narrow trail of permanent damage along the ion path called ion track [7,8]. Also, it produces point defects and defect clusters. In the recent years there has been a tremendous interest in the studies of phase transformation under SHI. A few researchers reported the phase transformation of single crystals, thin films and polycrystalline Y_2O_3 under energetic heavy ion irradiation [9,10]. In the present work, 120 MeV Ag^{9+} ion induced phase transformation of sol–gel synthesized nanocrystalline yttrium oxide is reported.

2. Materials and methods

Nanocrystalline yttrium oxide is synthesized by the sol gel technique using yttrium (III) nitrate hexahydrate ($Y(NO_3)_3{\cdot}6H_2O$ – Aldrich chemicals), citric acid anhydrous GR ($C_6H_8O_7$) and 25% GR ammonia solution (NH_3) (Merck specialties private limited). The ratio of citric acid/Y^{3+} is equal to 2. The detailed experimental procedure was discussed elsewhere [11]. Pellets (5 mm diameter and 1 mm thick) of Y_2O_3 are prepared by applying a pressure of

* Corresponding author.
E-mail address: bnlnarasappa@rediffmail.com (B.N. Lakshminarasappa).

http://dx.doi.org/10.1016/j.nimb.2016.04.013
0168-583X/

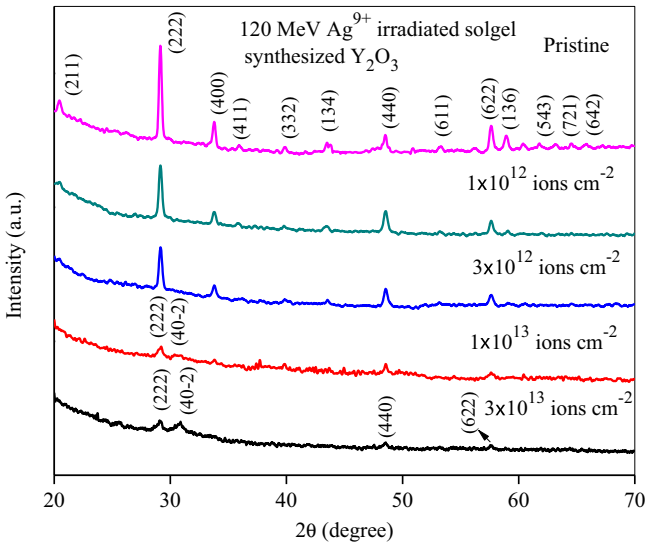

Fig. 1. X-ray diffraction patterns of pristine and 120 MeV swift Ag^{9+} ion irradiated Y_2O_3.

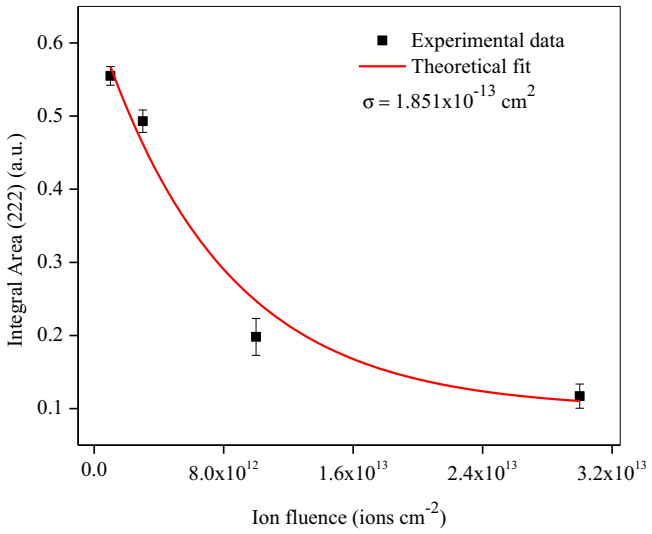

Fig. 2. Variation of integral area of (222) plane with ion fluences in Y_2O_3.

4 MPa using a homemade pelletizer. The pellets are annealed at 900 °C for 2 h in a muffle furnace. One of these pellets is kept as pristine and the others are irradiated with 120 MeV Ag^{9+} ions in the fluence range 1×10^{12}–3×10^{13} ions cm^{-2} at Inter University Accelerator Center, New Delhi, India.

The pristine and irradiated samples are characterized by X-ray diffraction (XRD) method [Bruker D8, using Cu-K_α radiation of wavelength 1.5406 Å]. The morphology and atomic structural information of the samples are studied by transmission electron microscopy (TEM) high resolution TEM (HR-TEM) and selected area electron diffraction (SAED) techniques [MIRA II LMH from TESCAN]. The powder sample of sol–gel synthesized Y_2O_3 is dispersed in ethanol for ~30 min and a drop was placed on the surface of a carbon-coated grid (300 mesh) to record TEM micrographs. Raman spectra are recorded in the range 200–1050 cm^{-1} using ID Raman micro-785 Ocean Optics microscope with an excitation wavelength of 785 nm.

3. Results and discussion

3.1. X-ray diffraction

XRD patterns of pristine and 120 MeV Ag^{9+} ion irradiated yttrium oxide are shown in Fig. 1. Pristine sample exhibits XRD peaks centered at 20.44°, 29.14°, 33.78°, 35.98°, 39.79°, 43.51°, 48.52°, 53.30°, 56.21°, 57.62°, 58.94°, 60.40° and 61.80° corresponding to (211), (222), (400), (411), (332), (134), (440), (611), (541), (622), (136), (444), (543) respectively. These planes are indexed to the cubic phase of Y_2O_3 with the space group $Ia\bar{3}$ (JCPDS No. 88-1040) [12]. At lower fluence (1×10^{12}–3×10^{12} ions cm^{-2}) 2θ positions of XRD lines closely match the values of pristine sample. However, the relative intensities are less due to loss of crystallinity with increase of ion fluence. Further, a weak and new diffraction peak at 30.36° is observed at a fluence 1×10^{13} ions cm^{-2}. This peak corresponds to the monoclinic phase with space group C2/m [9,10,13]. This peak is assigned to $(40\bar{2})$ plane (JCPDS 47-1274). The intensity of all the diffracted peaks of the cubic phase decreases with ion fluence where as the peak correspond to monoclinic phase $(40\bar{2})$ increases. Thus, integral intensity of all the diffraction peaks (cubic phase) exponentially decreases with increasing ion fluence. It is due to the fact that, ion irradiation leads to the damage of Y_2O_3 lattice and induces more number of oxygen vacancies, extended defects and internal stress in materials and these may also responsible of the phase transformation. A strong intense diffraction peak at 29.14° corresponds to (222) plane is selected for the analysis. The effect of ion fluence on integral intensity of 29.14° peak is fitted using by Poison equation [14,15]

$$I(\varphi) = I_0 \exp(-\sigma\varphi) \quad (1)$$

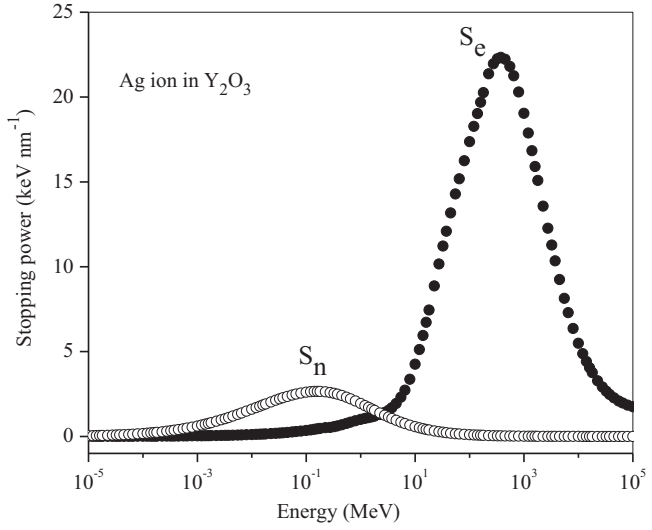

Fig. 3. Variation of electronic energy loss (S_e) and nuclear energy loss (S_n) for Ag ion in yttrium oxide target.

Table 1
Ion impact parameters.

Ions	Energy (MeV)	S_e (keV nm^{-1})	Range (μm)	Target type	References
Si^{8+}	100	4.103	21.65	Nanocrystal	Lakshminarasappa et al. [17]
Xe	0.38	18.0	–	Thin film	Gaboriaud et al. [15]
Ag^{9+}	120	18.270	11.10	Nanocrystal	Present work

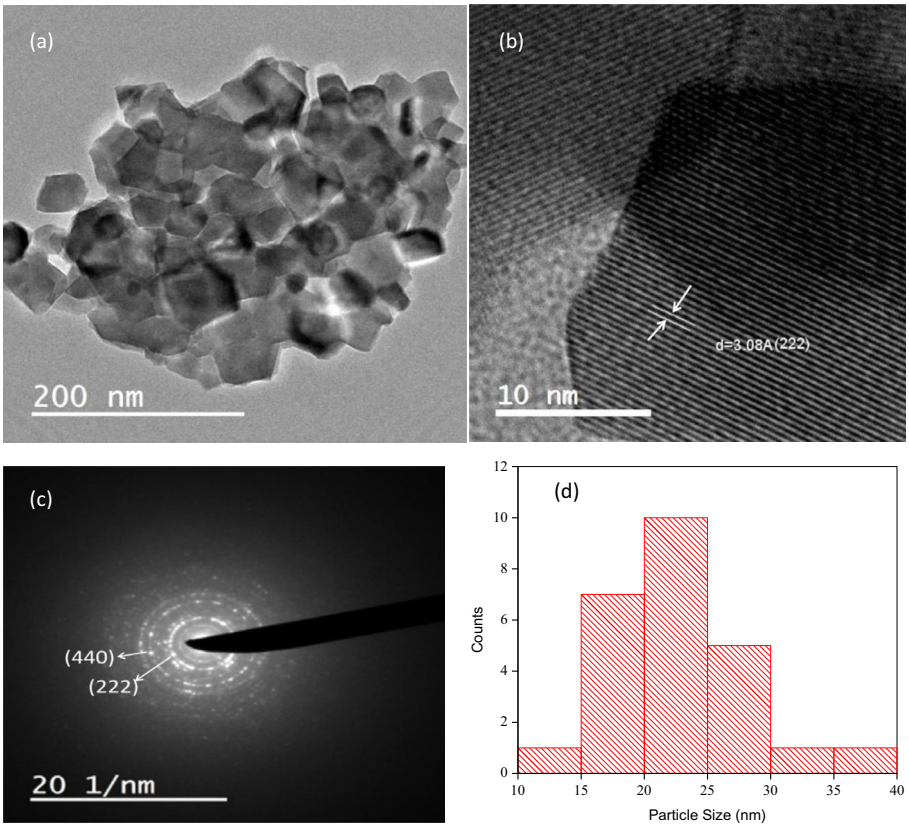

Fig. 4. (a) TEM micrograph, (b) HR-TEM micrograph (c) SAED pattern and (d) Size distribution histogram of pristine Y_2O_3 nanocrystals.

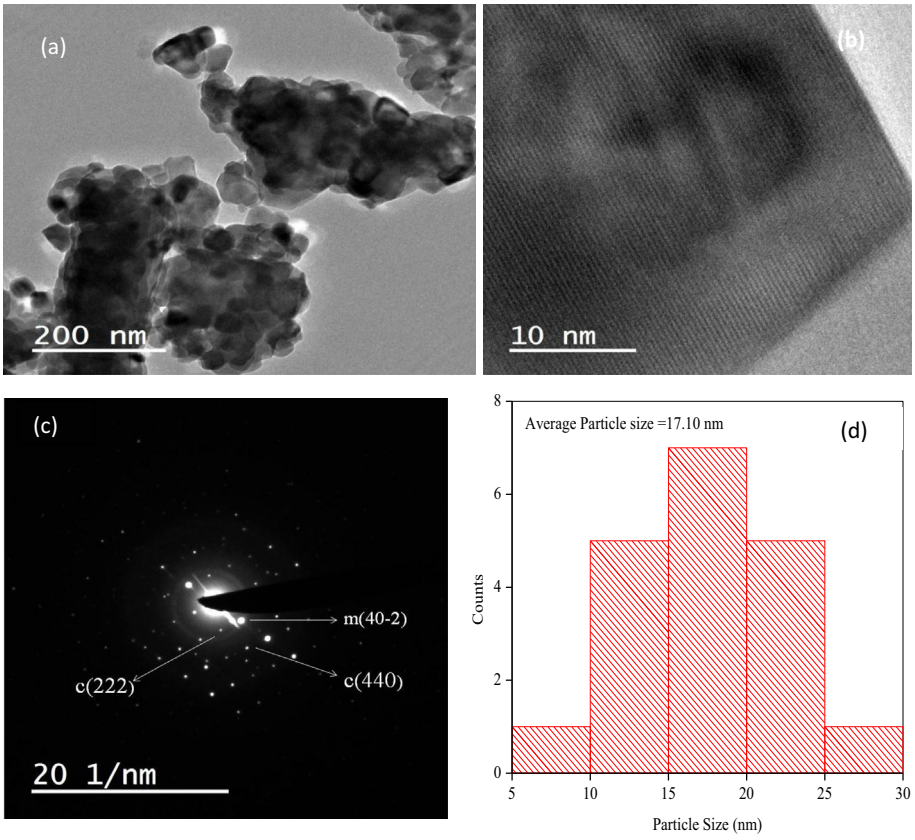

Fig. 5. (a) TEM micrograph, (b) HR-TEM micrograph (c) SAED pattern and (d) Size distribution histogram of 120 MeV Ag^{9+} (3×10^{13} ions cm^{-2}) irradiated Y_2O_3 nanocrystals.

where σ is the damage cross section of phosphor ($\sigma = \pi r^2$), r is the effective radius of ion track, I_0 is the integral area of pristine (222) plane sample, $I(\varphi)$ is the integral area of SHI irradiated sample with ion fluence φ. Fig. 2 shows integral area under the peak (222) as a function of ion fluence. It is found that, the integrated area decreases exponentially with ion fluence. The radius of the ion tracks is estimated by fitting this equation and it is found to be 2.43 nm.

The electronic energy loss (S_e), nuclear energy loss (S_n) and projected ion range (R_p) of 120 MeV Ag ions in Y_2O_3 are calculated using stopping and range of ions in matter (SRIM) software and is shown in Fig. 3 [16]. The obtained ion impact parameters are tabulated in Table 1. The threshold electronic energy loss (S_{eth}) for phase transformation in Y_2O_3 is 18 keV nm^{-1} [9]. Previously, it was not observed any phase transformation in 100 MeV Si^{8+} irradiated Y_2O_3 [11] where the value of Se (4.103 keV nm^{-1}) was much lower than that the present work (18.27 keV nm^{-1}). Hence, the phase transformation is observed in the present work due to higher Se value of Ag^{9+}ions in Y_2O_3 lattice. The phase transformation due to SHI irradiation is explained using the thermal spike model. According to thermal spike model the energy deposited by the heavy ions is diffused on the electrons. Then, the electrons transfer their energy to the lattice by the electron–atom interaction. Finally, the energy is diffused in the lattice and induces a local increase of lattice temperature in a cylindrical region around the ion path. This local heating followed by a rapid quenching may induce a phase transformation and/or loss of crystallinity [17].

3.2. TEM analysis

Crystal quality, particle size and detailed atomic structural information can be obtained by characterizing the nanocrystal using TEM, HR-TEM and SAED techniques. Figs. 4 and 5(a–c) shows the TEM, HR-TEM and SAED image of pristine and 120 MeV Ag^{9+} ion irradiated (3×10^{13} ions cm^{-2}) Y_2O_3 samples. Well separated and irregular shaped nanoparticles are observed in pristine Y_2O_3. Figs. 4 and 5(d) shows the size distribution histogram for the TEM images. The mean particle size for pristine Y_2O_3 and SHI samples are found to be 25 and 17 nm respectively. The size distribution analysis of the particles is carried out by scanning each image for 20–30 particles using the standard software 'Image Tool' [18]. It is clear that, the maximum number of particles occurs in size ranges 20–25 nm and 15–20 nm for pristine and ion irradiated Y_2O_3 respectively. Hence, it may be conclude that the synthesized material is nanocrystalline in nature and SHI irradiation induces loss of crystallinity.

HR-TEM image confirm that, the pristine sample exhibits cubic crystal system. It also indicates damage free lattice fringes with an estimated interplanar spacing of 0.308 nm that represents the (222) plane. Also, SAED pattern shows the planes at (222), (440) belongs to cubic crystal system. HR-TEM and SAED pattern of ion irradiated sample shows a new plane $(40\bar{2})$ correspond to monoclinic phase. The interplanar spacing of (222) (440) and $(40\bar{2})$ are found to be 0.308, 0.187 and 0.294 nm respectively. And also HR-TEM shows dark spots in irradiated samples because of reduction in particle size and larger number of defects [19,20] on the surface of the nanoparticles. Also, ion beam induces more damage and disorder to Y_2O_3 lattice. Therefore, SAED pattern show more diffraction spot.

3.3. Raman spectroscopy

Raman spectroscopy is a very sensitive technique and it provides information on vibration of molecules within the scattering volume. The vibration of optical modes in cubic Y_2O_3 are given [21] by

$$\Gamma_{op} = 4A_g + 4E_g + 14F_g + 5A_{zu} + 5E_u + 16F_u$$

where $4A_g$, $4E_g$ and $14F_g$ are Raman active, $16F_u$ is IR active and $5A_{zu}$, $5E_u$ are inactive modes. Thus, there are twenty two Raman active modes, where E_g and F_g modes are doubly and triply degenerated respectively. The Raman active modes of cubic Y_2O_3 can be divided into fifteen modes ($3A_g + 3E_g + 9F_g$) coming from the vibration of O ions and seven modes ($A_g + E_g + 5F_g$) coming from the vibration of Y ions [22]. Fig. 6(a) and (b) shows the Raman spectra of pristine and 120 MeV Ag^{9+} irradiated (3×10^{13} ions cm^{-2}) Y_2O_3. The observed Raman modes are tabulated in Table 2. It is clear that the strongest Raman peaks observed at 375 cm^{-1} for pristine and ion irradiated Y_2O_3. The major and high scattering intensity peak in the samples has been attributed to $F_g + E_g$ mode [22]. It indicates a large polarizability of vibration. This band is characteristic of the cubic structure and is observed in both pristine and ion irradiated samples. Raman peak intensity at 375 cm^{-1} is found to be decreased in ion irradiated sample. It is due to loss of crystallinity. As the crystallite size decreases the phonons are confined to the small volume of the particles. This leads to broadening of Raman

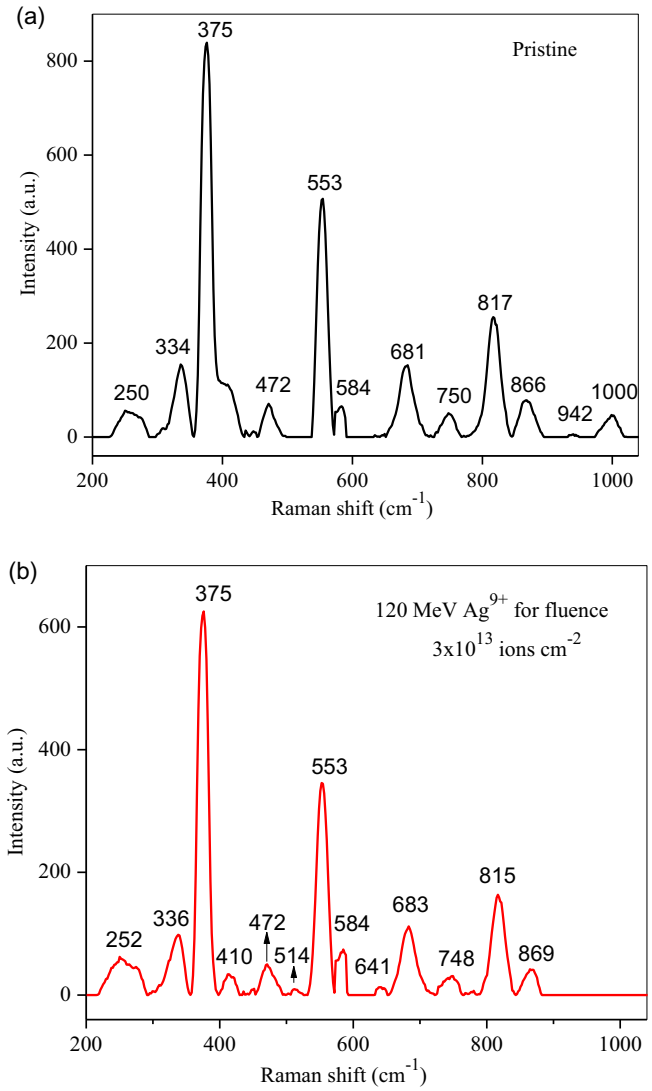

Fig. 6. Raman spectra of (a) pristine and (b) 120 MeV swift Ag^{9+} ion irradiated Y_2O_3 nanocrystals.

Table 2
Peak positions of Raman modes of pristine and 120 MeV swift Ag^{9+} (3×10^{13} ions cm^{-2}) ion irradiated Y_2O_3.

Modes of vibration	F_g	F_g	$F_g + E_g$		F_g		A_g	E_g		F_g	O–O	O–O	O–O	O–O	CF
Pristine	250	334	375	–	472	–	553	584	–	681	750	817	866	942	1000
3×10^{13} ions cm^{-2}	252	336	375	410	472	514	553	584	641	683	748	815	869	–	–

peaks. The broadening of the Raman peaks is attributed to reduction of particle size [14]. In an infinite crystal, only phonons near the center of the Brillouin zone contribute to the sharp Raman peaks due to momentum conservation between phonons and incident light. On the other hand, in a finite crystal, phonon can be confined by crystal boundaries or defects such as oxygen vacancies, which give raise to lattice strain and loss of stoichiometry. This result allowing phonons with the non-center of the Brillouin zone contribute to the broadening of Raman peaks [23]. Other Raman peaks intensities are decreased and shifted towards the higher wave number region indicating disorder in the system. New Raman peaks are also observed at 410, 514 and 641 cm^{-1}, these peaks are assigned to monoclinic phase [24]. Pristine sample shows peaks at 750, 817, 866, 942 and 1000 cm^{-1} are attributed to O–O stretching vibration [25,26] and crystal-field (CF) excitation [27]. Raman peaks at 942 and 1000 cm^{-2} are disappeared after SHI irradiation indicating change in crystal filed. This leads to rearrangement of atoms in a system resulting change of crystal system from cubic to monoclinic structure.

4. Conclusion

In summary, SHI induced phase transformations have been studied in nanocrystalline yttrium oxide. A new XRD peak appeared at 30.36° correspond to $(40\bar{2})$ plane confirm the monoclinic phase. Also TEM image confirmed the lattice damage and phase modification under SHI. The results indicate that the cubic to monoclinic transition involves a strong growth of the nanostructure due to the structural extended defects, it originating from the oxygen network behavior, which leads to polygonisation up to a nanocrystallite structure, followed by a phase transformation from cubic structure into a monoclinic structure. This is further confirmed by new Raman peaks observed at 410, 514 and 641 cm^{-1} corresponds to monoclinic structure.

Acknowledgements

The authors express their sincere thanks to Dr. D.K. Avasthi, Senior Scientist, Dr. P.K. Kulriya, Materials Science Group, IUAC, New Delhi, India for their constant encouragement and help during the experiment. Dr. Subramanyam, Ms. Usha, JNCSR, Bangalore, India for their help in recording TEM images and authors would like to thank DST PURSE program for providing the Raman spectroscopy measurement facility at Department of Physics, Bangalore University, Bangalore. Also, one of the authors (NJS) is grateful to Inter University Accelerator Centre, New Delhi, for providing fellowship under UFR (No. 48303) scheme.

References

[1] B. Yan, X.Q. Su, Opt. Mater. 29 (2007) 547.
[2] D.N. Patel, L.A. Hardy, T.J. Smith, E.S. Smith, D.M. Wright, S. Sarkisov, J. Lumin. 133 (2013) 114.
[3] J. Zhong, H. Liang, B. Han, X.Q. Su, T. Tao, Chem. Phys. Lett. 453 (2008) 192.
[4] A. Fukabori, M. Sekita, T. Ikegami, N. Iyi, T. Komatsu, M. Kawamura, M. Suzuki, J. Appl. Phys. 101 (2007) 043112.
[5] H. Huang, X. Sun, S. Wang, Y. Liu, X. Li, J. Liu, Z. Kang, S.T. Lee, Dalton Trans. 40 (2011) 11362.
[6] M.W. Barsoum, Fundamentals of Ceramics, McGraw-Hill Co., Inc., 1997, ISBN 978-0070055216, pp. 67–69.
[7] P. Kluth, C. Schnohr, O. Pakarinen, F. Djurabekova, D. Sprouster, R. Giulian, M. Toulemonde, Phys. Rev. Lett. 101 (2008) 175503.
[8] A. Benyagoub, Phys. Rev. B 72 (2005) 094114.
[9] R.J. Gaboriaud, M. Jublot, F. Paumier, B. Lacroix, Nucl. Instrum. Methods Phys. Res., Sect. B 310 (2013) 6.
[10] S. Hémon, C. Dufour, A. Berthelot, F. Gourbilleau, E. Paumier, S. Bégin-Collin, Nucl. Instrum. Methods Phys. Res., Sect. B. 166–167 (2000) 339.
[11] B.N. Lakshminarasappa, N.J. Shivaramu, K.R. Nagabhushana, F. Singh, Nucl. Instrum. Methods Phys. Res., Sect. B 329 (2014) 40.
[12] Tong. Liu, Xu. Wen, Xue. Bai, Hongwei. Song, J. Appl. Phys. 111 (2012) 064312.
[13] S. Hémon, V. Chailley, E. Dooryhée, C. Dufour, F. Gourbilleau, F. Levesque, et al., Nucl. Instrum. Methods Phys. Res., Sect. B 122 (1997) 563.
[14] S.K. Gautam, F. Singh, I. Sulania, R.G. Singh, P.K. Kulriya, E. Pippel, J. Appl. Phys. 115 (2014) 143504.
[15] R. Singhal, F. Singh, A. Tripathi, D.K. Avasthi, Radiat. Eff. Defects Solids. 164 (2009) 38.
[16] J.F. Ziegler, M.D. Ziegler, J.P. Biersack, SRIM the stopping and range of ions in matter, Nucl. Instrum. Methods Phys. Res., Sect. B 268 (2010) 1818.
[17] G. Schiwietz, K. Czerski, M. Roth, F. Staufenbiel, P.L. Grande, Nucl. Instrum. Methods Phys. Res., Sect. B 226 (2004) 683.
[18] N. Dilawar, D. Varandani, S. Mehrotra, H.K. Poswal, S.M. Sharma, A.K. Bandyopadhyay, Nanotechnology 19 (2008) 115703.
[19] M. Mitric, A. Kremenovic, R. Dimitrijevic, D. Rodic, Solid State Ionics 101 (1997) 495.
[20] Khorsand Zak, M.E. Abd. Majid, M.E. Abrishami, Ramin Yousefi, Solid State Sci. 13 (2011) 251.
[21] S. Bhagavantam, T. Venkataryudu, Proc. Indian Acad. Sci., Sect. A 9 (1939) 224.
[22] Sudeshna Ray, Sergio Fabian Leon-Luis, Francisco Javier Manjon, Miguel Alfonso Mollar, Oscar Gomis, Ulises Ruyman Rodríguez-Mendoza, Said Agouram, Alfonso Munoz, Victor Lavin, Cur. Appl. Phys. 14 (2014) 72.
[23] J. Zuo, C. Xu, Y. Liu, Nanostract. Mater. 10 (1999) 1331–1335.
[24] Stuart deutsch, High Pressure Phase Transformations In Polycrystalline Yttrium Oxide Ph.D thesis, 2012 (New Brunswick, New Jersey).
[25] J.S. Valentine, Chem. Rev. 73 (1973) 235.
[26] X.L. Jing, Q.C. Chen, C. He, X.Q. Zhu, W.Z. Weng, W.S. Xia, H.L. Wan, Phys. Chem. Chem. Phys. 14 (2012) 6898.
[27] J.F. Martel, S. Jandl, A.M. Lejus, B. Viana, D. Vivien, J. Alloys Compd. 353 (1998) 275.